Eur. Phys. J. A (2021) 57:233
https://doi.org/10.1140/epja/s10050-021-00548-y

THE EUROPEAN PHYSICAL JOURNAL A

Regular Article - Experimental Physics

Activation cross sections of gamma-emitters produced in deuteron induced reactions on ^{209}Bi up to 50 MeV

F. Tárkányi[1], S. Takács[1], F. Ditrói[1,a], Z. Szűcs[1], K. Brezovcsik[1], A. Hermanne[2], A. V. Ignatyuk[3]

[1] Institute for Nuclear Research (ATOMKI), Debrecen, Hungary
[2] Cyclotron Laboratory, Vrije Universiteit Brussel (VUB), Brussels, Belgium
[3] Institute of Physics and Power Engineering (IPPE), Obninsk, Russia

Received: 24 March 2021 / Accepted: 30 June 2021 / Published online: 14 July 2021

Communicated by Aurora Tumino

Abstract Deuteron induced reactions on natural bismuth targets were investigated with the stacked foil activation technique up to 50 MeV. Excitation functions for the reactions ^{209}Bi(d,xn)^{207,206,205}Po, Bi(d,x)^{207,205}Bi and ^{209}Bi(d,x)^{203}Pb obtained from gamma-spectra of decay products were compared with the results of our ALICE-D and EMPIRE-D model calculations, with the result of TALYS code taken from TENDL-2019 on-line library and the results of the only measurement performed earlier. Thick target yields were deduced from the fitted experimental cross sections.

1 Introduction

We perform a systematic investigation of the activation cross-sections of deuteron induced nuclear reactions in all elements since years. The investigation has covered 65 elements (individual stable isotopes or elemental targets with natural isotopic composition): Be, B, C, N, Ne, Mg, Al, Si, Sc, Ti, V, Cr, Mn, Fe, Co, Ni, Cu, Zn, Ga, Ge, Se, Kr, Rb, Sr, Y, Zr, Nb, Mo, Ru, Rh, Pd, Ag, Cd, In, Sn, Sb, Te, Xe, Cs, Ba, La, Ce, Pr, Nd, Sm, Eu, Gd, Tb, Dy, Ho, Er, Tm, Yb, Lu, Hf, Ta, W, Re, Os, Ir, Pt, Au, Hg, Tl and Pb. The investigations are connected to different projects on activation analyses, medical isotope production, radiation safety of accelerator elements, nuclear reaction theory and more. In the present work we investigated the activation cross-sections on bismuth up to 50 MeV deuteron energy. Lead-bismuth eutectics are under consideration as a target material with high-energy protons and deuterons for generating spallation neutrons and for nuclear coolant material in reactor technology. For this purposes deuteron activation cross-sections are already collected in the Fusion Evaluated Data Library (FENDL-3 library [1]), presently based mainly on results of TALYS model calculations.

A throughout literature survey resulted in only one experimental dataset on ^{209}Bi for production cross-sections of gamma-emitter radionuclides by Gonchar et al. [2], studying the deuteron induced reactions up to 47 MeV incident particle energy. In our earlier study of alpha particle induced reactions on Bi (Hermanne et al. [3]) we investigated both gamma and alpha particle emitting reaction products. In the present study we had studied only the activation cross sections of radionuclides with gamma emission.

2 Experiment and data evalution

For determination of the cross section data the activation method, by using stacked-foil target technique and off-line gamma-ray spectrometry were used. The bismuth targets were prepared by vacuum evaporation onto Al backing. The surface thickness of the Bi layer of each target was determined by measuring the weight of the foils before and after evaporation of the bismuth layer. The average thickness of the evaporated bismuth layers was about 1.8 μm. The thickness of the Al-backings was 51 μm, and 13 mm in diameter. The diameter of the evaporated spot was 8 mm. The evaporated samples were ordered according to their Bi-weight and the smallest and highest weight samples were paired and created an Al-Bi-Al sandwiched target putting the bismuth layers face-to-face. This way 20 bismuth targets were created with an overall Bi layers of 2.5–3.7 μm. The Al backings served as recoil catchers and as monitor foils for exact determination of beam parameters (intensity and energy) along the stack. Additionally, 102.6 μm thick Al energy degrader foils were inserted into the high energy part of the stack and 10.9 μm

[a] e-mail: ditroi@atomki.hu (corresponding author)

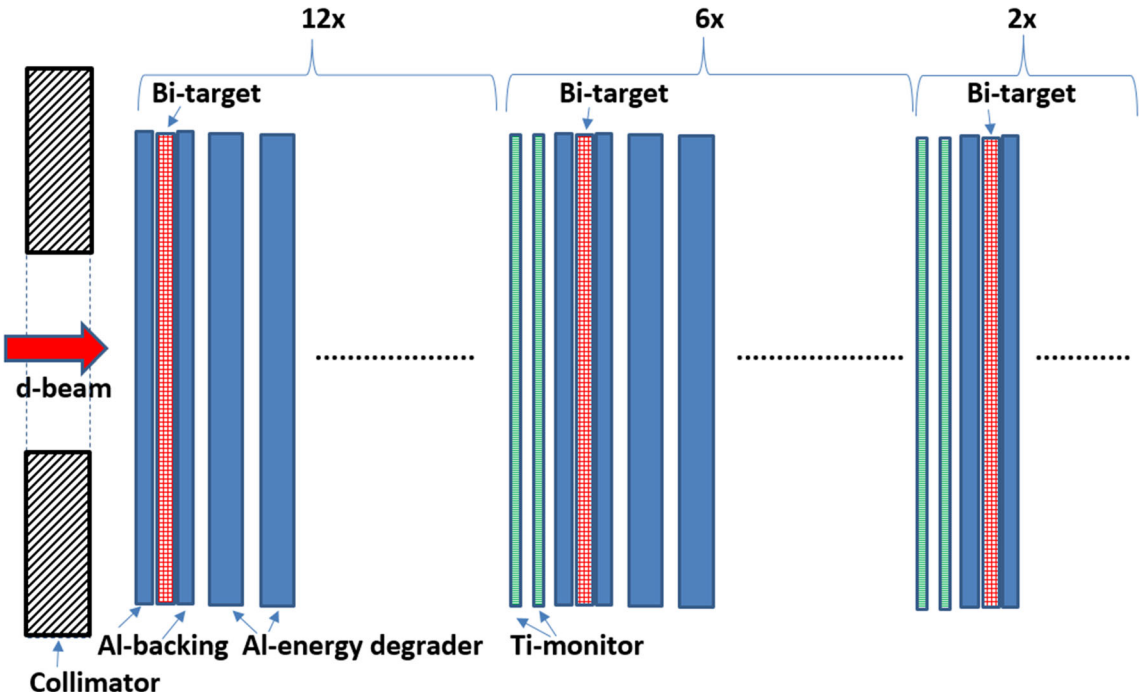

Fig. 1 Target-stack composition (the foil thicknesses are shown in Table 1)

Ti foils for beam monitoring in the low energy segment of the stack (see Fig. 1).

The stacked target was irradiated in a Faraday cup like target holder equipped with a collimator of 3 mm in diameter, which determined beam size. The beam current was kept constant at about 20 nA during the 40 min irradiation. The details of the target stack, the experimental technique and the data evaluations are summarized in Table 1. The decay data used in data analysis are collected in Table 2. Effective beam intensities and the energy scale were determined by using the excitation functions of the ^{24}Al(d,x)^{22,24}Na and ^{nat}Ti(d,x)^{48}V monitor reactions. The excitation functions of these reactions, in comparison with the IAEA recommended data for monitors [4] are shown in Fig. 2. For estimation of the uncertainty of the effective beam energy in the target foils, cumulative effects of possible uncertainties in primary energy and target thickness were taken into account together with the effect of the energy straggling and of the correction for the monitor reaction (0.3–1.1 MeV). The uncertainties of cross sections were obtained from the sum in quadrature of all individual contributions (beam current (7%), beam-loss corrections (maximum 1.5%), target thickness (3%), detector efficiency (5%), photo peak area determination and counting statistics (1–20%) [5]. The main individual source of the uncertainties is the uncertainty of the counting statistics. The uncertainties of the non-linear contributing time related processes and parameters were not considered.

The activities of the detected radioisotopes were calculated from the spectrometry of the corresponding gamma-lines (Eq. 1) [6]:

$$A_{EOB} = \frac{T}{\varepsilon I_\gamma t_{live}} \frac{\lambda t_{real}}{1 - e^{\lambda t_{real}}} e^{-\lambda t_c} \tag{1}$$

where A_{EOB} denotes the activity at End of Bombardment (EOB), T is the net count in the gamma-peak, λ is the decay constant, t_{real}, t_{live} and t_c are the real-time, live-time of the measurement and the cooling time, respectively I_γ is the gamma-line absolute intensity and ε is the detector efficiency. From the activities the corresponding cross section was calculated by using Eq. 2.

$$\sigma\,(E) = \frac{A_{EOB} M z e}{I\,(1 - e)\,\varrho s N_A v} \tag{2}$$

where z denotes the projectile charge, $I\,(A)$is the beam current, $N_A$is Avogadro's number (6.02214×10^{23} mol^{-1}), M (g/mol) is the molar mass of the chemical compound forming the target material, $e$is the electron charge (1.6×10^{-19} C), ρ(g/cm^3)is the density of the target material, s (cm) is the thickness of the target foil, ν is the number of atoms of the target element in the molecule and. $\sigma(E)$(cm^2)is the cross section at E median energy in the particular foil in the stack.

When complex particles are emitted instead of individual protons and neutrons the Q-values have to be decreased by the respective binding energies of the compound particles: np-d, +2.2 MeV; 2np-t, +8.48 MeV; n2p-^{3}He, +7.72 MeV; 2n2p-α, +28.30 MeV.

Table 1 Main experimental parameters and data evaluation

Experimental parameters		Data evaluation	
Incident particle	Deuteron	Gamma spectra evaluation	Genie 2000 [7]
			Forgamma [8]
Method	Stacked-foil	Determination of beam intensity	Faraday cup (preliminary)
			Fitted monitor reaction (final) [9]
Foil thickness	Bi target (3.8–2.5 μm)	Decay data	NUDAT 2.8 [10]
	Al_b backing (51 μm)		
	Al_e energy absorber (102.6 μm)		
	Ti monitor (10.9 μm)		
Number of Bi samples	20	Reaction Q-values	Q-value calculator [11]
Stack composition (Fig. 1)	Al_b-Bi-Al_b-Al_e-Al_e 12 times	Determination of beam energy	Andersen (preliminary) [12]
	Ti-Ti-Al_b-Bi-Al_b-Al_e-Al_e 6 times	Fitted monitor reaction (final) [4]	
	Ti-Ti-Al_b-Bi-Al_b 2 times		
Accelerator	Cyclone 110 cyclotron Université Catholique Louvain la Neuve (LLN)	Uncertainty of energy	Cumulative effects of possible uncertainties
Primary energy (MeV)	50	Cross-sections	Elemental cross-section
Energy range (MeV)	49.77–7.15	Uncertainty of cross sections	Sum in quadrature of all individual linear contributions [5]
Irradiation time (min)	40	Yield	Physical yield [13,14]
Beam current (nA)	20		
Monitor reactions, [recommended values]	$^{27}Al(d,x)^{24,22}Na$ [4] $^{nat}Ti(d,x)^{48}V$ [4]		
detector	HPGe		
γ-spectra measurements	4 series		
Cooling times (h)	7.2–10.5		
	44.4–52.3		
	133.4–221.2		
	13605–14389		

3 Nuclear model calculations

The cross sections of the investigated reactions were calculated using the modified pre-compound model codes ALICE-IPPE (Dityuk et al. [15]) and EMPIRE-II (Herman et al. [16]). To achieve better description of available data in the used ALIC-IPPE-D and in the EMPIRE-II-D a phenomenological enhancement factor K in these relations was taken as energy dependent and estimated to describe the whole set of the observed (d,p) cross sections for medium and heavy nuclei. The experimental data are also compared with the cross section data in the TENDL-2019 (Koning et al. [17]) nuclear reaction data library. The TENDL-2019 is based on both default and adjusted TALYS [18] calculations. In order to make the results comparable, the default options have been used with each model. Because the models are not perfect, they give results with different accuracy for different reactions. By using the same parameters (default), our results may help to the model developers to improve their description of processes.

Table 2 Decay and nuclear characteristics of the investigated reaction products, contributing reactions and their thresholds (used gammas are underlined)

Nuclide Spin	Half-life	Decay path (%)	E_γ (keV)	I_γ (%)	Contributing process	Q-value (keV)
^{207}Po	5.80 h	α: 0.021	405.78	9.70	^{209}Bi(d,4n)^{207}Po	−20262.0
$5/2^-$		ε: 99.979	742.72	28.4		
			911.77	17.0		
			992.39	59.2		
			1148.47	5.81		
^{206}Po	8.8 day	α: 5.45	286.410	22.9	^{209}Bi(d,5n)^{206}Po	−27291.0
0^+		ε: 94.55	338.44	18.5		
			522.47	15.1		
			807.38	21.8		
			1032.26	31.7		
^{205}Po	1.74 h	α: 0.040	261.0	4.0	^{209}Bi(d,6n)^{205}Po	−36029.0
$5/2^-$		ε: 99.960	836.8	19.2		
			849.8	25.5		
			872.4	37.0		
			1001.2	28.8		
^{207}Bi	31.55 year	ε: 100	569.698	97.75	^{209}Bi(d,p3n)^{207}Bi	−16571.0
$9/2^-$			1063.656	74.5	^{207}Po decay	−20262.0
^{205}Bi	15.31 day	ε: 100	570.60	4.34	^{209}Bi(d,p5n)^{207}Bi	−31704.0
$9/2^-$			579.80	5.44	^{205}Po decay	−36029.0
			703.45	31.1		
			987.66	16.1		
			1043.75	7.51		
^{203}Pb	51.92 h	ε: 100	279.195	80.9	^{209}Bi(d,α4n)^{203}Pb	−15047.0
$5/2^-$			401.320	3.35	^{203}Bi decay	−47386.0

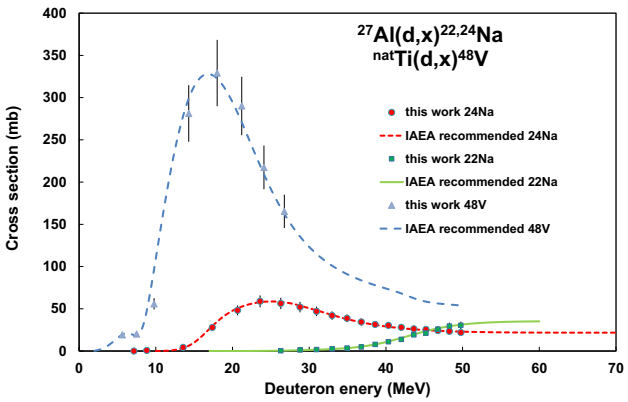

Fig. 2 Cross sections of monitor reactions for determination of deuteron beam energy and intensity

4 Results

4.1 Production cross sections

The measured experimental cross-section data are shown in Figs. 3, 4, 5, 6, 7 and 8 together with the results of the earlier measurement and of the theoretical calculations. The numerical values are presented in Tables 3 and 4.

The ^{209}Bi(d,4n)^{207}Po process

The new and literature cross sections for production of ^{207}Po (5.80 h, α: 0.021 %, ε: 99.979 %) in comparison with the model calculations are shown in Fig. 3. The agreement with the earlier data of Gonchar et al. [2] is excellent. Up to 40 MeV the TENDL data are closest to the experimental results. ALICE-D gives better approximation above 40 MeV and the maxima given by ALICE-D and EMPIRE-D are shifted down and up, respectively.

The ^{209}Bi(d,5n)^{206}Po process (Fig. 4)

The ^{206}Po (8.8 days, α: 5.45 %, ε: 94.55 %) is produced via the (d,5n) reaction. Our new results are in good agreement with the earlier experimental data [2], except of a couple of points, which also contradict to each other in the two series of literature data from the same author. Best agreement is seen with the TENDL prediction again. The maxima of ALICE-D and EMPIRE-D are shifted again in the same way as in the case of ^{207}Po.

Table 3 Cross sections of deuteron induced reactions on ^{209}Bi for production of ^{207,206,205}Po radionuclei

E	dE	^{207}Po		^{206}Po		^{205}Po	
		σ	dsig	σ	dsig	σ	dsig
(MeV)		mb					
49.77	0.30	278.8	34.8	599.9	75.0	420.6	53.5
48.28	0.33	309.4	38.3	731.5	91.9	275.1	36.9
46.77	0.35	325.2	40.3	810.1	100.8	161.1	26.0
45.23	0.38	355.9	43.7	891.4	110.8	82.8	15.8
43.64	0.41	394.6	48.6	833.2	103.5		
42.01	0.44	457.1	56.1	792.4	99.3		
40.33	0.47	553.5	67.5	690.2	87.7		
38.59	0.50	681.8	82.8	525.1	68.1		
36.79	0.53	816.7	99.0	298.2	41.7		
34.92	0.56	924.2	111.9	132.5	24.8		
32.98	0.59	920.6	111.5				
30.95	0.63	848.8	103.3				
28.80	0.67	600.6	74.2				
26.30	0.71	220.0	29.0				

Table 4 Cross sections of deuteron induced reactions on ^{209}Bi for production of ^{207,205}Bi, ^{203}Pb radionuclei

E	dE	^{207}Bi		^{205}Bi		^{203}Pb	
		σ	dsig	σ	dsig	σ	dsig
(MeV)		mb					
49.77	0.30	635.7	76.9	327.2	39.4	13.3	1.8
48.28	0.33	606.9	73.3	221.5	27.1	10.8	1.6
46.77	0.35	622.8	75.5	130.0	16.3	9.6	1.5
45.23	0.38	643.8	77.7	95.1	12.1	7.2	1.3
43.64	0.41	632.5	77.9	28.7	4.6	5.1	1.1
42.01	0.44	705.9	85.4	4.3	2.1	2.9	0.4
40.33	0.47	793.1	97.0				
38.59	0.50	941.2	113.8				
36.79	0.53	1079.2	130.6				
34.92	0.56	1155.7	139.6				
32.98	0.59	1113.2	135.7				
30.95	0.63	1080.4	130.8				
28.80	0.67	810.4	98.5				
23.60	0.77	63.0	13.0				

The ^{209}Bi(d,6n)^{205}Po process (Fig. 5).

No earlier experimental data were found for production of ^{206}Po (1.74 h, α: 0.040 %, ε: 99.960 %). The theoretical data differ significantly from each other in magnitude, but in our measuring energy region this difference is not so significant. Our new data are between the TENDL and EMPIRE-D predictions.

The ^{209}Bi(d,x)^{207}Bi process (Fig. 6)

The measured cumulative cross sections for production of long-lived ^{207}Bi (31.55 y, ε: 100 %) were deduced after complete decay of the ^{207}Po parent (5.80 h, α: 0.021 %, ε: 99.979 %). No earlier data were reported for cumulative cross section. Gonchar et al. [2] reported only direct production data (2 data points). Cumulative cross sections were deduced by us from his ^{207}Po parent and ^{207}Bi direct data and are in perfect agreement with our measurement. The TENDL description is more close to the experimental data than the other model calculations.

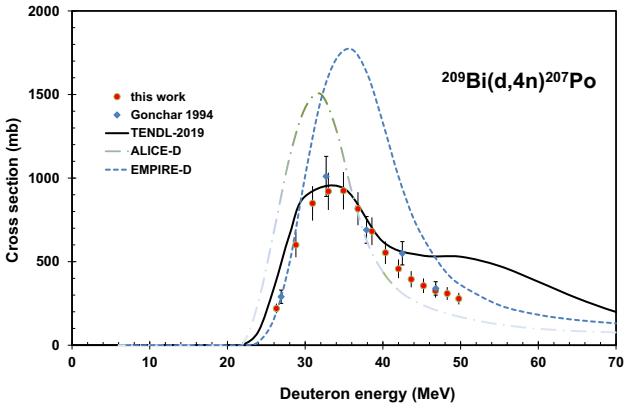

Fig. 3 Experimental and theoretical excitation functions for the ^{209}Bi(d,4n)^{207}Po reaction

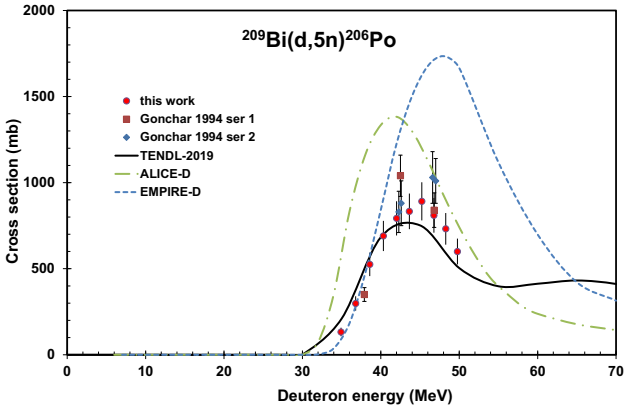

Fig. 4 Experimental and theoretical excitation functions for the ^{209}Bi(d,5n)^{206}Po reaction

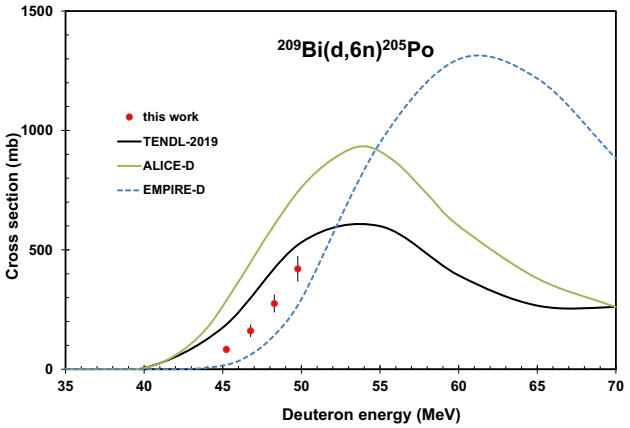

Fig. 5 Experimental and theoretical excitation functions for the ^{209}Bi(d,4n)^{205}Po reaction

The ^{209}Bi(d,x)^{205}Bi process (Fig. 7)

The measured production cross-sections of ^{205}Bi (15.31 days, ε: 100 %) are cumulative, deduced from spectra

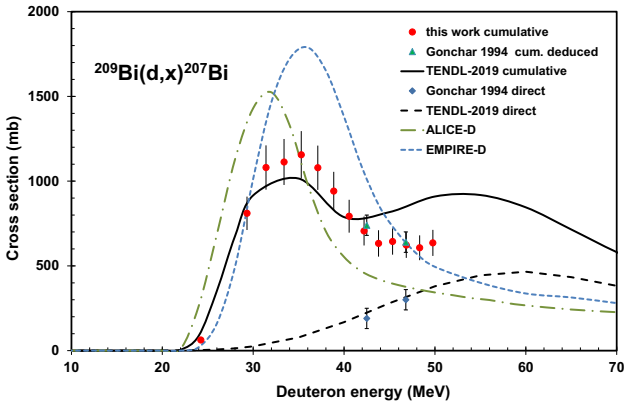

Fig. 6 Experimental and theoretical excitation functions for the ^{209}Bi(d,x)^{207}Bi reaction

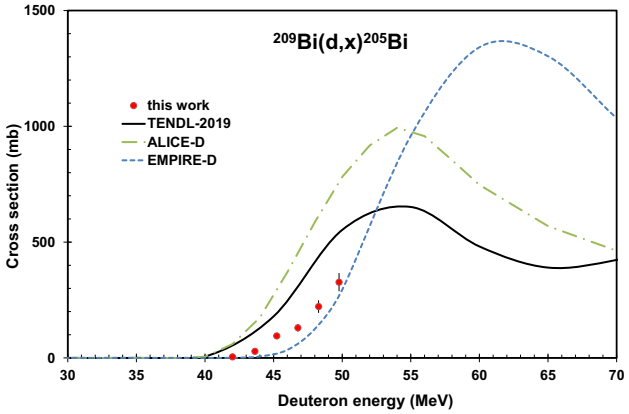

Fig. 7 Experimental and theoretical excitation functions for the ^{209}Bi(d,x)^{205}Bi reaction

obtained after complete decay of its ^{205}Po parent (1.74 h, α: 0.040 %, ε: 99.960 %). No earlier experimental data were found for production of ^{205}Bi. The magnitude and the position of the maximum cross-sections of the model calculations are very different but in the limited energy region of our measurements the results are near to the EMPIRE-D predictions.

The ^{209}Bi(d,x)^{203}Pb process (Fig. 8)

The results could in principle be cumulative but in practice the possible contribution of the very small alpha decay of ^{207}Po (5.80 h, α: 0.021 %, ε: 99.979 %) has to be neglected and no ^{203}Pb activity was detected around 30 MeV, at the maximum cross section of ^{207}Po. Also possible contribution of the decay from ^{203}Bi (11.76 h, ε: 100 %) can start only from higher energy as the threshold for the ^{209}Bi(d,6n) reaction is Q= -45597.0 keV. Our experimental data are hence due to the ^{209}Bi(d,α4n)^{203}Pb reaction with Q = −15047.0 keV. No earlier data were found in literature. The three theoretical models show large disagreement in their predictions.

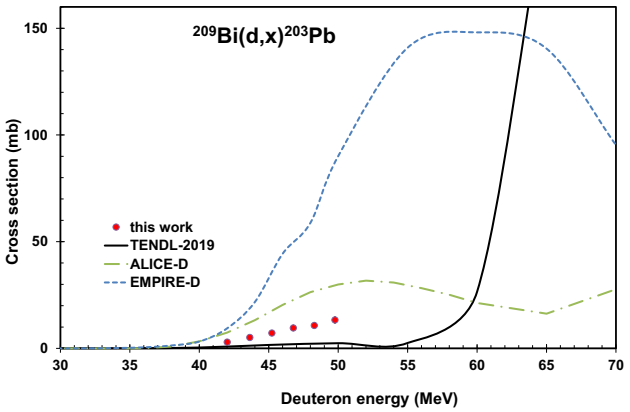

Fig. 8 Experimental and theoretical excitation functions for the ^{209}Bi(d,x)^{203}Pb reaction

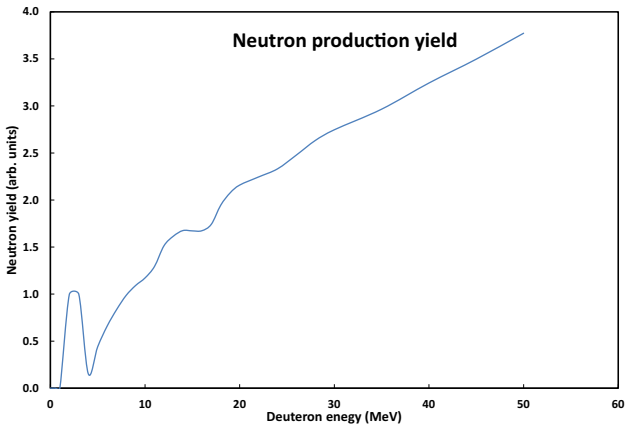

Fig. 9 Neutron production yield by bombarding ^{209}Bi target with 50 MeV deuterons, calculated by the TENDL-2019 on-line library

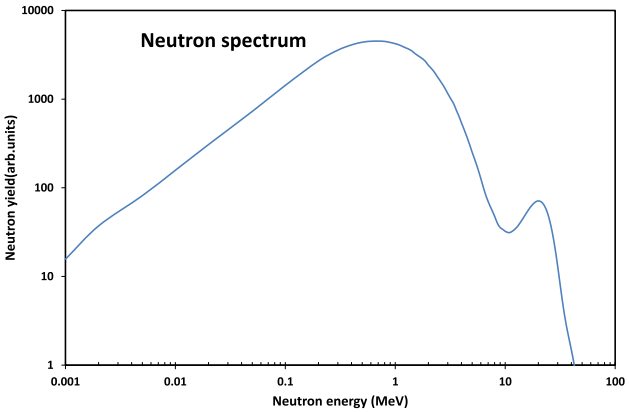

Fig. 10 Neutron energy spectrum by bombarding ^{209}Bi target with 50 MeV deuterons, calculated by the TENDL-2019 on-line library

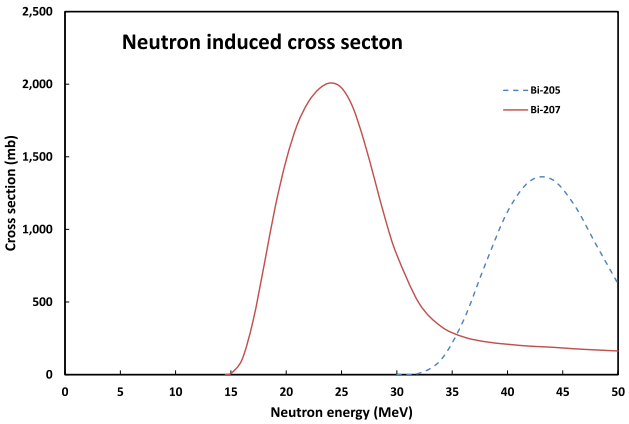

Fig. 11 Cross sections of the neutron induced reactions ^{209}Bi(n,x)^{205,207}Bi

Contribution of secondary neutron contribution

As usual by deuteron bombardment of heavy elements a lot of neutrons are produced in the nuclear reaction of direct, pre-equilibrium, compound, stripping, knock-out, break-up, etc. processes. We used the TENDL-2019 on-line library to demonstrate the effects might arise from secondary neutrons. In Fig. 9. The total production yield of neutrons is shown originating from of all nuclear reactions of 50 MeV deuteron bombardment. In order to discuss the possible effect of secondary neutrons we must now the energy distribution of them. A typical neutron spectrum is seen in Fig. 10 also taken from the TENDL-2019 library.

In principle these neutrons might give contribution to our cross sections via the ^{209}Bi(n,x)^{205,207}Bi reactions. The estimated excitation functions of these neutron induced reactions on natural bismuth are shown in Fig. 11. It is obvious from the neutron spectrum in Fig. 10. that only a small fraction of the produced neutrons has an energy above the thresholds of the ^{209}Bi(n,x)^{205,207}Bi reactions (29.6 and 14.4 MeV, respectively).

In order to completely exclude the neutron contribution a short and simple calculation can be made by estimating the number of secondary neutrons. The number of reactions (number of produced nuclei) can be calculated according to Eq. 3.

$$N\,(t) = N_t N_b \sigma \tag{3}$$

Where $N(t)$ is the number of produced nuclei (number of reactions occurred) versus time, N_t is the number of target nuclei (^{209}Bi) as layer thickness (atom/cm^2),N_b is the number of bombarding particles (1/s), σ (cm^2) is the cross section and. By using Eq. 3. and supposing 1 μA beam current, 1 μm target thickness and an average cross section of 100 mb (overestimation), the number of deuteron induced reactions producing heavy products and neutrons is 1.6 10^9/s/μA/μm.

The ratio of the number of neutrons and the numbers of the deuterons of 1μA deuteron beam is 2.8 10^{-3}. Taking a cross section for the neutron induced reactions an order of magnitude higher (overestimation, 1000 mb), the same number of target atoms and the number of neutrons, estimated above

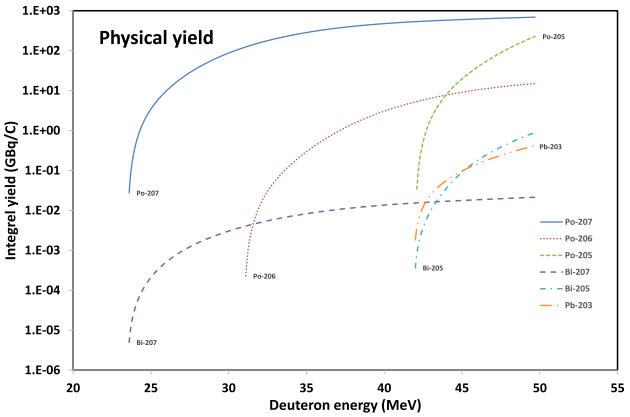

Fig. 12 Integral yields of the ^{209}Bi(d,xn)^{207,206,205}Po, ^{209}Bi(d,x)^{207,205}Bi,^{203}Pb reactions calculated from the measured excitation functions

the contribution by secondary neutrons is about two orders of magnitude less than that for the deuterons. Regarding the energy distribution of the secondary neutrons and the threshold energies of the corresponding two reactions only a very small fractions of the secondary neutrons are capable to contribute to the production of the ^{205,207}Bi radionuclides. Estimating the fraction of high energy neutrons, we found that less than 8% of the secondary neutrons have enough energy for producing ^{207}Bi and less than 0.5% for producing ^{205}Bi radionuclides. By combining these two values with production rate of the secondary neutrons it turns out that contributions of the secondary neutrons for the formation of ^{205,207}Bi is five to six orders of magnitude lower than the deuteron induced part. This small effect of the secondary neutrons is unmeasurable and therefore can be neglected. The secondary neutrons from the parts of the beam transport system, based on our earlier experiences, were not taken into account.

5 Integral yields

The experimental points were fitted (spline fit) and integral thick target yields were calculated according to the definition given by Otuka et al. [14]. The yields are shown in Fig. 12. No earlier experimental data on ^{209}Bi(d,x) have been found in the literature.

6 Summary

In the frame of a systematic investigation of activation cross sections of deuteron induced reactions new experimental cross-sections were measured for the ^{209}Bi(d,xn)^{207,206,205}Po, ^{209}Bi(d,x)^{207,205}Bi and ^{209}Bi(d,αn)^{203}Pb reactions up to 50 MeV deuteron energy and compared with the earlier experimental data of Gonchar et al. [2]. Excellent agreement was found with the literature values, both in energy scale and cross-section values, for the ^{209}Bi(d,xn)^{207,206}Po, ^{209}Bi(d,x)^{207}Bi reactions. No earlier data were reported for ^{209}Bi(d,xn)^{205}Po, ^{209}Bi(d,x)^{205}Bi and ^{209}Bi(d,αn)^{203}Pb reactions. To test the predictivity of the nuclear reaction models, the measured excitation functions were compared to the results obtained with our calculations using ALICE-IPPE –D and EMPIRE-D theoretical codes and the theoretical results of TALYS code taken from TENDL-2019 library. The predictions of the model codes among themselves are significantly different and differ from experimental data.

Acknowledgements This work was done in the frame of MTA-FWO (Vlaanderen) research projects. The authors acknowledge the support of research projects and of their respective institutions in providing the materials and the facilities for this work. This work was also partly supported (F. Ditrói) by IAEA RER Project 1020 and by IAEA CRP F22069.

Funding Open access funding provided by ELKH Institute for Nuclear Research.

Data Availability Statement This manuscript has associated data in a data repository. [Authors' comment: The associated data of this manuscript will be deposited in the EXFOR on-line Nuclear Data Library (https://www-nds.iaea.org/exfor/exfor.htm) after publication of this paper.]

References

1. IAEA, FENDL-3.0: Fusion Evaluated Nuclear Data Library Ver.3.0, https://www-nds.iaea.org/fendl30/data/deuteron, IAEA, Vienna (2015). Accessed 11 Jan 2021
2. A.V. Gonchar, S.N. Kondratyev, Y.N. Lobach, S.V. Nevsky, V.D. Sklyarenko, V.V. Tokarevsky, Integral cross sections for (d, xn) and (d, pxn) reactions on Bi-209 nuclei at deuteron energy range to 47 MeV. Izv. Rossiiskoi Akademii Nauk Ser. Fiz. **58**, 81–86 (1994)
3. A. Hermanne, F. Tárkányi, S. Takács, Z. Szucs, Y.N. Shubin, A.I. Dityuk, Experimental study of the cross-sections of alpha-particle induced reactions on Bi-209. Appl. Radiat. Isot. **63**, 1–9 (2005)
4. A. Hermanne, A.V. Ignatyuk, R. Capote, B.V. Carlson, J.W. Engle, M.A. Kellett, T. Kibedi, G. Kim, F.G. Kondev, M. Hussain, O. Lebeda, A. Luca, Y. Nagai, H. Naik, A.L. Nichols, F.M. Nortier, S.V. Suryanarayana, S. Takacs, F.T. Tarkanyi, M. Verpelli, Reference cross sections for charged-particle monitor reactions. Nucl. Data Sheets **148**, 338–382 (2018)

5. International-Bureau-of-Weights-and-Measures, Guide to the expression of uncertainty in measurement, 1st ed. International Organization for Standardization, Genève, Switzerland. ISBN 9267101889 (1993)
6. F. Tárkányi, A. Hermanne, F. Ditrói, S. Takács, A.V. Ignatyuk, I. Spahn, S. Spellerberg, Activation cross section data of deuteron induced nuclear reactions on rubidium up to 50 MeV. Eur. Phys. J. A **57**, 21 (2021)
7. Canberra, http://www.canberra.com/products/radiochemistry_lab/genie-2000-software.asp., (2000). Accessed 6 June 2021
8. G. Székely, Fgm—a flexible gamma-spectrum analysis program for a small computer. Comput. Phys. Commun. **34**, 313–324 (1985)
9. F. Tárkányi, F. Szelecsényi, S. Takács, Determination of effective bombarding energies and fluxes using improved stacked-foil technique. Acta Radiol. Suppl. **376**, 72 (1991)
10. A.A. Sonzogni, NuDat 2.0: Nuclear Structure and Decay Data on the Internet, http://www.nndc.bnl.gov/nudat2, in: M.B.C.e. Robert C. Haight (ed.) , Toshihiko Kawano (ed.) , Patrick Talou (ed.) (Ed.) ND2004—International Conference on Nuclear Data for Science and Technology, AIP Conference Proceedings, September 26 - October 1, 2004, Santa Fe, New Mexico, USA, pp. 547–577 (2005)
11. B. Pritychenko, A. Sonzogni, *Q-Value Calculator* (NNDC, Brookhaven National Laboratory, 2003)
12. H.H. Andersen, J.F. Ziegler, *Hydrogen stopping powers and ranges in all elements. The stopping and ranges of ions in matter*, vol. 3 (Pergamon Press, New York, 1977)
13. M. Bonardi, The contribution to nuclear data for biomedical radioisotope production from the Milan cyclotron facility, in *Consultants Meeting on Data Requirements for Medical Radioisotope Production, IAEA, INDC(NDS)-195 (1988)*. ed. by K. Okamoto (Tokyo, Japan, 1987), pp. 98–112
14. N. Otuka, S. Takács, Definitions of radioisotope thick target yields. Radiochim. Acta **103**, 1–6 (2015)
15. A.I. Dityuk, A.Y. Konobeyev, V.P. Lunev, Y.N. Shubin, *New Version of the Advanced Computer Code ALICE-IPPE, INDC (CCP)-410* (IAEA, Vienna., 1998)
16. M. Herman, R. Capote, B.V. Carlson, P. Oblozinsky, M. Sin, A. Trkov, H. Wienke, V. Zerkin, EMPIRE: Nuclear reaction model code system for data evaluation. Nucl. Data Sheets **108**, 2655–2715 (2007)
17. A.J. Koning, D. Rochman, J.C. Sublet, N. Dzysiuk, M. Fleming, S. van der Marck, TENDL-2019, https://tendl.web.psi.ch/tendl_2019/tendl2019.html (2019). Accessed 19 Mar 2021
18. A.J. Koning, D. Rochman, Modern nuclear data evaluation with the TALYS code system. Nucl. Data Sheets **113**, 2841–3172 (2012)